Journal of Geodesy (2019) 93:1123–1136
https://doi.org/10.1007/s00190-019-01230-4

ORIGINAL ARTICLE

Galileo and QZSS precise orbit and clock determination using new satellite metadata

Xingxing Li[1,2] · Yongqiang Yuan[1] · Jiande Huang[1] · Yiting Zhu[1] · Jiaqi Wu[1] · Yun Xiong[1] · Xin Li[1] · Keke Zhang[1]

Received: 18 January 2018 / Accepted: 13 January 2019 / Published online: 2 February 2019

Abstract
During 2016–2018, satellite metadata/information including antenna parameters, attitude laws and physical characteristics such as mass, dimensions and optical properties were released for Galileo and QZSS (except for the QZS-1 optical coefficients). These metadata are critical for improving the accuracy of precise orbit and clock determination. In this contribution, we evaluate the benefits of these new metadata to orbit and clock in three aspects: the phase center offsets and variations (PCO and PCV), the yaw-attitude model and solar radiation pressure (SRP) model. The updating of Galileo PCO and PCV corrections, from the values estimated by Deutsches Zentrum für Luft- und Raumfahrt and Deutsches GeoForschungsZentrum to the chamber calibrations disclosed by new metadata, has only a slight influence on Galileo orbits, with overlap differences within only 1 mm. By modeling the yaw attitude of Galileo satellites and QZS-2 spacecraft (SVN J002) according to new published attitude laws, the residuals of ionosphere-free carrier-phase combinations can be obviously decreased in yaw maneuver seasons. With the new attitude models, the 3D overlap RMS in eclipse seasons can be decreased from 12.3 cm, 14.7 cm, 16.8 cm and 34.7 cm to 11.7 cm, 13.4 cm, 15.8 cm and 32.9 cm for Galileo In-Orbit Validation (IOV), Full Operational Capability (FOC), FOC in elliptical orbits (FOCe) and QZS-2 satellites, respectively. By applying the a priori box-wing SRP model with new satellite dimensions and optical coefficients, the 3D overlap RMS are 5.3 cm, 6.2 cm, 5.3 cm and 16.6 cm for Galileo IOV, FOCe, FOC and QZS-2 satellites, with improvements of 11.0%, 14.7%, 14.0% and 13.8% when compared with the updated Extended CODE Orbit Model (ECOM2). The satellite laser ranging (SLR) validation reveals that the a priori box-wing model has smaller mean biases of −0.4 cm, −0.4 cm and 0.6 cm for Galileo FOCe, FOC and QZS-2 satellites, while a slightly larger mean bias of −1.0 cm is observed for Galileo IOV satellites. Moreover, the SLR residual dependencies of Galileo IOV and FOC satellites on the elongation angle almost vanish when the a priori box-wing SRP model is applied. As for satellite clocks, a visible bump appears in the Modified Allan deviation at integration time of 20,000 s for Galileo Passive Hydrogen Maser with ECOM2, while it almost vanishes when the a priori box-wing SRP model and new metadata are applied. The standard deviations of clock overlap can also be significantly reduced by using new metadata.

Keywords Precise orbit determination · Galileo · Quasi-Zenith Satellite System (QZSS) · Phase center offsets and variations · Yaw attitude · Solar radiation pressure (SRP)

1 Introduction

Currently, GPS and GLONASS are both operating at full capability and are also being gradually modernized. Over the past decades, the International GNSS Service (IGS; Dow et al. 2009) has made continuous efforts to advance the quality of orbit and clock products for GPS and GLONASS. Several critical issues have been well studied for GPS and GLONASS precise orbit determination (POD) and precise clock estimation (PCE), including phase center offsets and variations (PCO and PCV; Schmid et al. 2005, 2007), yaw-attitude models (Bar-Sever 1994; Kouba 2008, 2013; Dilssner 2010; Dilssner et al. 2011; Montenbruck et al. 2015a) and solar radiation pressure (SRP) models (Beutler et al. 1994; Bar-Sever and Kuang 2004; Arnold et al. 2015). Final combined precise orbit and clock products of GPS (and orbit

✉ Xingxing Li
lxlq109121@gmail.com

[1] School of Geodesy and Geomatics, Wuhan University, 129 Luoyu Road, Wuhan 430079, Hubei, China

[2] German Research Centre for Geosciences (GFZ), Telegrafenberg, 14473 Potsdam, Germany

products of GLONASS) have been generated and provided by IGS.

Next to GPS and GLONASS, Galileo has presently 26 satellites including 4 In-Orbit Validation (IOV) and 22 Full Operational Capability (FOC) satellites. The full Galileo constellation is scheduled to be accomplished in 2020 with 30 satellites. The Japanese Quasi-Zenith Satellite System (QZSS), which aims to build a regional navigation/augmentation service, has become a four-satellite constellation in 2017 to serve Asia-Oceania regions. Efforts will be made to establish a seven-satellite QZSS constellation in the future. For the new Galileo and QZSS constellations, several orbit modeling issues, including PCO/PCV, yaw attitude and SRP modeling, still need further investigations.

Due to the non-publication of pre-launch calibration values of Galileo satellites, conventional PCO values were adopted for IOVs (Montenbruck et al. 2014) and preliminary estimated PCO values were used for FOCs (Steigenberger et al. 2015) in the early studies (Montenbruck et al. 2015a; Schmid et al. 2015). In 2016, PCO values for IOV and FOC satellites were estimated by two different analysis centers (Deutsches Zentrum für Luft- und Raumfahrt, DLR and Deutsches GeoForschungsZentrum, GFZ; Steigenberger et al. 2016), and the averaged DLR/GFZ PCO solution can reduce the orbit day-boundary discontinuities by up to one-third. However, PCVs were ignored in precise Galileo processing because of the non-publication of consolidated PCV estimates or calibrations.

The yaw-attitude models of GPS and GLONASS were presented by Kouba (2008) and Dilssner et al. (2011). However, nominal attitude was used for Galileo IOV and FOC due to limited knowledge about elaborate yaw-attitude laws. As a result, increased orbit fit RMS values are observed for all types of Galileo satellites in eclipse seasons (Steigenberger and Montenbruck 2016). QZS-1 has two different attitude modes (yaw steering, YS and orbit normal, ON) depending on the β angle (Ishijima et al. 2009), and Hauschild et al. (2012) reported that the switch over from YS to ON takes place prior to the threshold of $|\beta| = 20°$.

The Extended CODE Orbit Model (ECOM; Beutler et al. 1994; Springer et al. 1999), developed by Center for Orbit Determination in Europe (CODE), is the most widely used SRP model for routine processing of GPS orbits (Guo et al. 2016). However, ECOM model has problems with precisely representing the orbits of new GNSS satellites, and could introduce large draconitic error in GNSS geodetic products (Meindl et al. 2013; Rodríguez-Solano et al. 2014). As a result, ECOM2 model, an updated version of ECOM, was developed by Arnold et al. (2015), and has been used by CODE for orbit processing since early 2015 (Dach et al. 2016). Compared to ECOM, ECOM2 uses the orbit angle with respect to orbit noon as angular argument, and has higher-order harmonics in the Sun-direction. The orbit accuracy of Galileo and QZSS can be improved using ECOM2 instead of ECOM (Prange et al. 2017). Considering the cuboidal shape of Galileo satellites, Montenbruck et al. (2015b) introduced an a priori model to ECOM for IOV satellites POD to mitigate obvious SRP modeling deficits. This model, known as Cuboid Box-Wing (CBW), is also appropriate for Galileo FOC satellites (Steigenberger and Montenbruck 2016). Zhao et al. (2017) introduced a CBW model for QZS-1 reducing the systematic orbit errors. The deficiencies of Galileo and QZSS SRP modeling still exist due to limited knowledge about the satellites, e.g., dimensions and optical properties of the satellite surfaces.

Fortunately, the new metadata of Galileo and QZSS satellites were published by the European GNSS Service Centre (EGSC) and the Cabinet Office (CAO), Government of Japan during 2016–2018 (EGSC 2017; CAO 2017, 2018). These new information, including antenna parameters (PCOs and PCVs), the attitude laws and physical characteristics such as mass, dimensions and optical properties, provide us a great opportunity to improve the orbit and clock modeling. In this contribution, we will evaluate the benefits of these new metadata for Galileo and QZSS POD and PCE. Our paper is organized as follows. After this introduction, current Galileo and QZSS constellations and tracking networks are overviewed in Sect. 2. In Sect. 3, several updates in POD with new metadata are described and the POD processing strategies are summarized. In Sect. 4, the Galileo and QZSS POD performances using new metadata are evaluated, followed by the analysis of satellite clock performances in Sect. 5. The conclusions and discussions are provided in Sect. 6.

2 Galileo and QZSS constellations and tracking network

2.1 Current Galileo and QZSS constellations

By November 2018, the Galileo constellation consists of 4 IOV and 22 FOC satellites. The four IOV satellites were brought into orbit in 2011 and 2012, and one of them (E20) experienced a sudden power loss in May 2014 (de Selding 2014) and thus is assigned a "Not Available" status (https://www.gsc-europa.eu/system-status/Constellation-Information). The first two FOC satellites (E18 and E14) were launched in August 2014, but they were injected into elliptical orbits with an inclination about 5° smaller than planned. These two FOC satellites are labeled as "FOCe" in this study (Steigenberger and Montenbruck 2016). According to the Notice Advisory to Galileo Users (NAGU) information #2017045 (available at https://www.gsc-europa.eu/notice-advisory-to-galileo-users-nagu-2017045), another FOC satellite E22 was removed from active service since December 8, 2017, until further notice

for constellation management purposes. The latest four FOC satellites were launched on July 25, 2018, and they are still under commissioning. A total of 17 Galileo satellites are used in this study, including 3 IOV, 2 FOCe and 12 FOC satellites. The two satellites E11 and E22 are running on Rubidium Atomic Frequency Standards (RAFSs), while the remaining 15 satellites are running on Passive Hydrogen Masers (PHMs).

The QZSS consists of three Inclined Geosynchronous Orbit (IGSO) satellites and one Geostationary Earth Orbit (GEO) satellite. The first IGSO satellite was launched in 2010, and the other two IGSO and one GEO satellites were launched in 2017. Only QZS-1 and QZS-2 (SVNs J001 and J002) are studied in this contribution, since the observations for QZS-3 and QZS-4 (SVNs J003 and J004) during the study period are insufficient for long-time analysis.

2.2 Galileo and QZSS tracking network

IGS has initiated the Multi-GNSS Experiment (MGEX) project in 2012 to collect and analyze data of emerging new signals and systems (Montenbruck et al. 2017). By DOY (Day of Year) 310 of 2017, there are totally 230 MGEX stations available at the FTP server of the Crustal Dynamics Data Information System (CDDIS), including 203 stations tracking both Galileo IOV and FOC, 61 stations tracking QZS-1 and 58 stations tracking QZS-2. All QZSS-enabled stations are employed in this study, and most of them can also track Galileo satellites. Besides, 49 additional Galileo-capable stations are selected carefully to complete the distribution shown in Fig. 1. It is clear that most QZSS stations are located in Asia-Oceania regions.

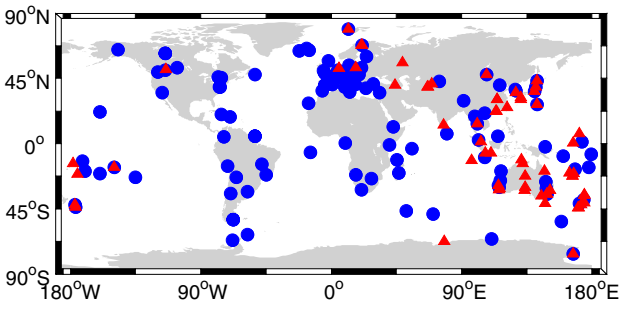

Fig. 1 Distribution of tracking stations selected for Galileo and QZSS POD. The blue circles are for stations with Galileo capacity, and the red triangles are for QZSS

3 New metadata and POD strategy

3.1 Galileo and QZSS metadata

3.1.1 Antenna Metadata

The navigation antenna onboard each Galileo satellite has been chamber-calibrated prior to launch. However, the calibration results were not available until the publication of the Galileo satellite metadata. As a result, conventional values of $(x, y, z)_{\mathrm{IGS}} = (-0.2, 0.0, +0.6)$ m and $(x, y, z)_{\mathrm{IGS}} = (+0.15, 0.0, +1.0)$ m for the transmit antenna's center of phase w.r.t. the satellite's center of mass were recommended for Galileo IOV and FOC satellites, respectively, until GPS week 1914. Since GPS week 1915, PCOs estimated by GFZ and DLR in form of E1/E5a ionosphere-free linear combination (listed in Table 1) were included in IGS ANTEX (the Antenna Exchange Format) files. However, PCVs of IOV and FOC satellites were ignored.

The pre-launch chamber-calibrated PCO and PCV for Galileo IOV satellites were disclosed in December 2016, and the FOC values were added in October 2017 (EGSC 2017). The E1/E5a ionosphere-free metadata PCOs are listed in Table 2, while azimuth- and zenith-dependent PCVs are provided in the Galileo ANTEX file (https://www.gsc-europa.eu/sites/default/files/sites/all/files/ANTEX_GAL_FOC_IOV.atx). When compared with the estimated values in Table 1, significant differences of several decimeters can be found in the z-component, while the horizontal PCOs

Table 1 E1/E5a ionosphere-free PCO corrections of Galileo satellites (estimated by GFZ and DLR) and L1/L2 ionosphere-free PCO corrections of QZS-1 (Kogure 2012) in IGS ANTEX Reference Frame

Satellite type	x (mm)	y (mm)	z (mm)
Galileo IOV	−170	30	950
Galileo FOCe	160	−10	1050
Galileo FOC	120	−10	1100
QZS-1	−0.90	2.90	3514.77

Table 2 E1/E5a ionosphere-free PCO corrections of Galileo satellites and L1/L2 ionosphere-free PCO corrections of QZSS satellites provided by new metadata in IGS ANTEX Reference Frame

Satellite type	x (mm)	y (mm)	z (mm)
Galileo IOV	−174 to −168	32–35	823–924
Galileo FOCe	169–175	−14 to −13	864–908
Galileo FOC	113–122	−11 to −6	753–948
QZS-1	−1.10	1.60	3516.21
QZS-2	3.00	−1.90	1134.62

only differ slightly. It is worth noting that these chamber-calibrated PCOs and PCVs for the IOV satellites have been already included in the IGS ANTEX files since GPS week 1972, while these for the FOC satellites were added in GPS week 1986. Here, to study the influence of PCO and PCV corrections on Galileo POD, two sets of PCO/PCVs are compared, i.e., DLR/GFZ values with only PCO corrections and new metadata values with chamber-calibrated PCO and PCV corrections.

As for QZSS satellites, the PCOs of all four satellites and the PCVs of three satellites (QZS-1 PCV is not available) are given by CAO (2017, 2018). The PCOs of QZS-1 from these new published metadata are nearly the same as those from Kogure (2012) with a difference of (0.2, 1.3, 1.4) mm. In this study, the applied PCO corrections are listed in Table 2, and the PCVs are also corrected except QZS-1.

3.1.2 Attitude Modeling

The new metadata also provide the detailed attitude law, which is critical for attitude modeling during eclipse seasons. The nominal yaw steering formulas of both Galileo and QZSS satellites are expressed by:

$$\psi_{\text{nom}} = a\tan 2(\tan\beta, -\sin\mu) \tag{1}$$

where ψ_{nom} is the nominal yaw angle, β is the elevation of the Sun above the particular orbital plane and μ is the geocentric orbit angle between satellite and orbit midnight. $a$tan2 is the usual FORTRAN function of $\tan^{-1}$ giving signed angles between $(-\pi, \pi)$. The sign of the yaw angle is always the same as that of β in the case of Galileo and QZSS. When the Sun is close to the orbital plane ($\beta \approx 0°$), while the satellite approaches the orbit noon ($\mu \approx 180°$) or midnight ($\mu \approx 0°$), the nominal yaw-turn rate may exceed the respective maximum satellite hardware rates.

For Galileo IOV satellites, when $|\beta| < 2°$ and the satellite approaching orbit noon or midnight, an auxiliary Sun $\vec{S}_H$ is used to keep the yaw change rate low (EGSC 2017). With the approximation of $\cos\beta \approx 1$ when $|\beta| \approx 0$, the regions where the auxiliary Sun is used are simplified as:

$$\begin{aligned} &|\beta| < 2° \\ &|\mu| < 15° \text{ or } |\mu - 180°| < 15° \end{aligned} \tag{2}$$

For FOC satellites, the yaw-attitude maneuver takes place when:

$$\begin{aligned} &|\beta| < 4.1° \\ &|\mu| < 9.1° \text{ or } |\mu - 180°| < 9.1° \end{aligned} \tag{3}$$

The modified yaw angle depends on the elapsed time t_{mod} since the maneuver beginning (EGSC 2017):

$$t_{\text{mod}} = \frac{\mu - \mu_{\text{init}}}{\dot{\mu}} \tag{4}$$

where μ_{init} is the initial orbital angle at the maneuver beginning. $\dot{\mu}$ is the average orbital angular velocity that can be obtained by

$$\begin{aligned} \dot{\mu} &= \sqrt{\frac{GM}{a^3}} \\ a &= \frac{r}{2 - \frac{rv^2}{GM}} \end{aligned} \tag{5}$$

where $GM = 3.986004418 \times 10^{14}\ \text{m}^3\text{s}^{-2}$ is the geocentric gravitational constant, r and v are the position and velocity of the satellite, respectively. In this study, the standard FOC attitude model is also used for FOCe satellites E14 and E18.

The yaw-attitude angles during noon-turn (*left*) and midnight-turn of Galileo IOV and FOC satellites under approximate zero β angles are shown in Fig. 2. In the new yaw-attitude model, the slew rate is much smaller when passing the orbital noon and midnight. For IOV satellite E11, the noon-turn lasts for about 68 min (with $\beta \approx 0.27°$), and the midnight-turn lasts for about 70 min (with $\beta \approx 0.50°$). The difference between the nominal and modeled yaw angles can reach up to a maximum of 49° for noon-turn and 36.5° for midnight-turn. For FOC satellite E26, the full time of noon-turn and midnight-turn are both about 43 min, and the maximum difference between the nominal and actual yaw angles are 81.3° and 68.7° for noon- and midnight-turn, respectively.

Different from Galileo satellites, two attitude control modes of YS and ON are used by QZS-1. The switches from YS to ON mode and vice versa take place when $|\beta|$ is about 20°. In addition, ON mode is also used for orbital maneuvers. QZS-2 takes always the YS mode except orbital maneuver periods, and the yaw motion is planned to keep the maximum rate $\dot{\psi}$ of 0.055°/s and cross the nearest orbital noon or midnight when the Sun elevation angle is within 5°. The yaw angle coincides with the nominal at the beginning and the end of midnight- and noon-turns. Continuous ON mode is followed by the GEO satellites QZS-3, and the attitude law for QZS-4 is the same to that of QZS-2.

For QZS-2/4, the start and exit epochs of midnight- and noon-turns need to be solved iteratively. In this study, the initial orbit angles of start and exit epochs (μ_s and μ_e) are set to:

$$\begin{cases} \mu_s = -7°, \quad \mu_e = 7° \text{ midnight} \\ \mu_s = 173°, \quad \mu_e = -173° \text{ noon} \end{cases} \tag{6}$$

Then, the yaw angles (ψ_s and ψ_e) at the maneuver start and exit can be obtained by Eq. (1). The updating formulas for μ_s and μ_e are

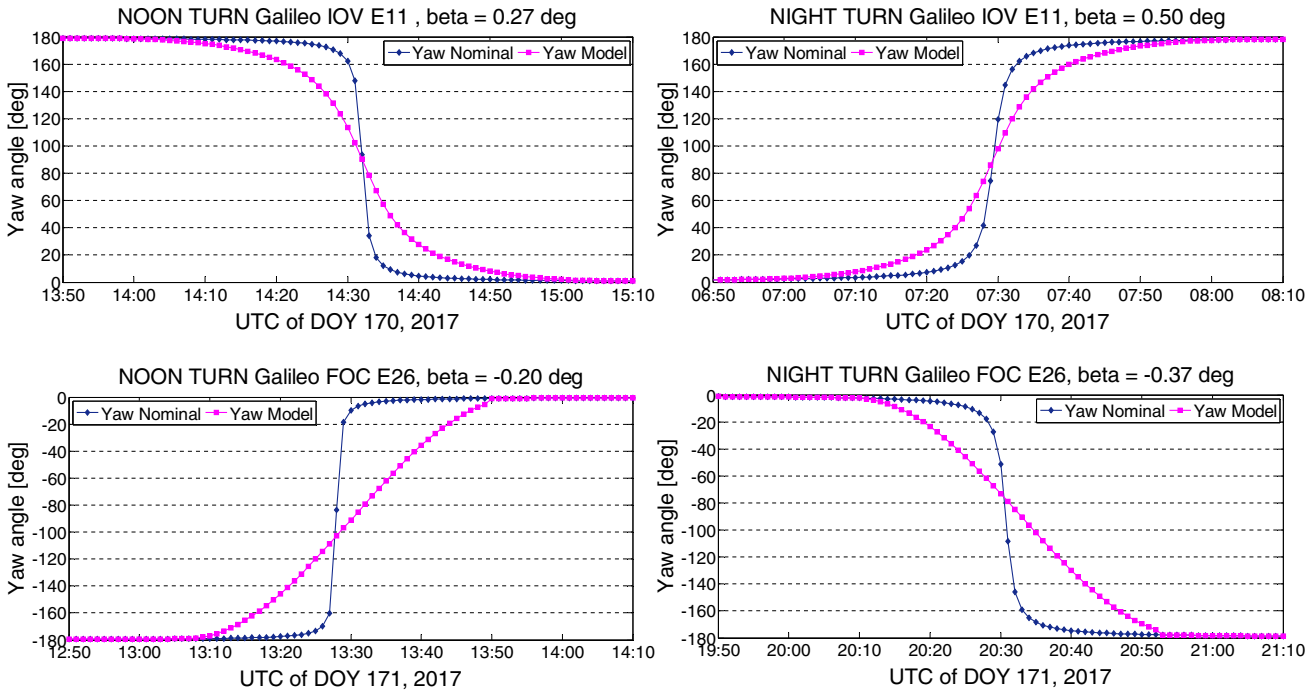

Fig. 2 Yaw-attitude angles during noon-turn (left) and midnight-turn (right) maneuver of Galileo IOV E11 (June 19, 2017) and Galileo FOC E26 (June 20, 2017). The blue rhombuses represent nominal yaw-attitude angles, and the magenta squares represent modeled yaw-attitude angles

$$\begin{cases} \mu_s = \dfrac{\dot{\mu}}{\dot{\psi}}\left(\mathrm{abs}(\psi_s) - \dfrac{\pi}{2}\right) \\ \mu_e = \dfrac{\dot{\mu}}{\dot{\psi}}\left(\mathrm{abs}(\psi_e) - \dfrac{\pi}{2}\right) \end{cases} \quad \text{For midnight - turn}$$

$$\begin{cases} \mu_s = \dfrac{\dot{\mu}}{\dot{\psi}}\left(\mathrm{abs}(\psi_s) - \dfrac{\pi}{2}\right) + \pi \\ \mu_e = \dfrac{\dot{\mu}}{\dot{\psi}}\left(\mathrm{abs}(\psi_e) - \dfrac{\pi}{2}\right) + \pi \end{cases} \quad \text{For noon - turn} \tag{7}$$

The rotational direction R and the modified yaw angle $\psi_{\mathrm{QZS,\,mod}}$ are given by

$$R = \mathrm{SIGN}(1,\ \psi_e - \psi_s)$$
$$\psi_{\mathrm{QZS,\,mod}} = \psi_s + R \cdot \dot{\psi} \cdot \frac{\mu - \mu_s}{\dot{\mu}} \tag{8}$$

where SIGN(a, b) is the usual FORTRAN function returning the value of a with the sign of b.

Figure 3 shows the yaw-attitude angles during noon-turn (left) and midnight-turn of QZS-2 under approximate zero β angles. The noon-turn starts about 27 min before orbital noon and lasts for about 54 min (with $\beta \approx -0.20°$), and the midnight-turn starts about 26 min before orbital midnight and lasts for about 51 min (with $\beta \approx -0.57°$). The maximum

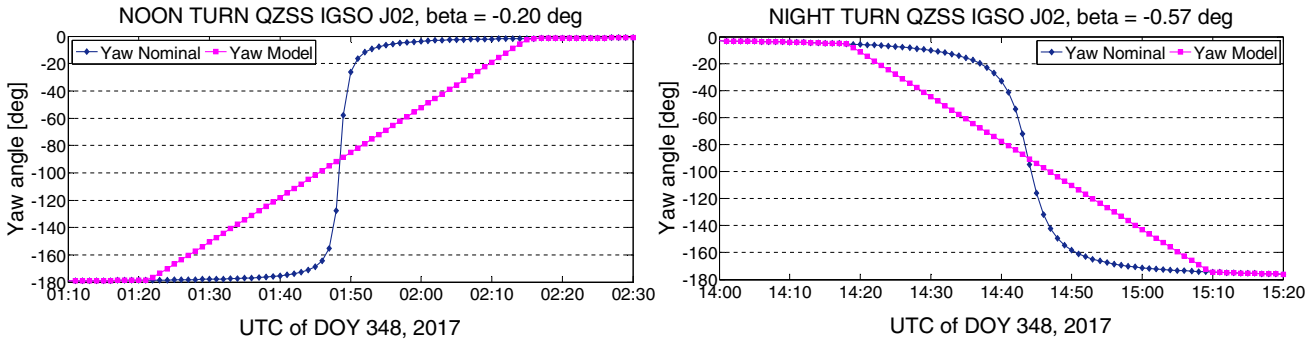

Fig. 3 Yaw-attitude angles during noon-turn (left) and midnight-turn (right) maneuver of QZS-2 (December 14, 2017). The blue rhombuses represent nominal yaw-attitude angles, and the magenta squares represent modeled yaw-attitude angles

difference between the nominal and actual yaw angles are 67.1° and 48.0° for noon- and midnight-turn, respectively.

3.1.3 SRP Modeling

Due to the limited information about satellite dimensions and optical properties, purely empirical models are widely used for SRP modeling. Whereas ECOM performs well for GPS, deficiencies appear when processing GLONASS, Galileo, BDS and QZSS (Prange et al. 2016). Arnold et al. (2015) updated ECOM to ECOM2, by using Δu as the angular argument instead of the argument of latitude u, and adding second- and fourth-order harmonic terms to D component (pointing from the satellite to the Sun):

$$\begin{aligned} a_D &= D_0 + D_{C2} \cdot \cos 2\Delta u + D_{S2} \cdot \sin 2\Delta u \\ &\quad + D_{C4} \cdot \cos 4\Delta u + D_{S4} \cdot \sin 4\Delta u \\ a_Y &= Y_0 \\ a_B &= B_0 + B_C \cdot \cos \Delta u + B_S \cdot \sin \Delta u \end{aligned} \tag{9}$$

where $\Delta u = u - u_S$ is used as the angular argument, with u_S being the argument of latitude of the Sun projected on the orbital plane.

As the detailed satellite dimensions and optical properties of Galileo and QZS-2 were released in the metadata, an a priori box-wing model is proposed in this study:

$$a = a_{\text{box-wing}} + a_{\text{emp}}. \tag{10}$$

The five-parameter ECOM (Springer et al. 1999) is used and estimated as a_{emp} on top of $a_{\text{box-wing}}$. The a priori box-wing acceleration $a_{\text{box-wing}}$ can be divided into the contributions of satellite body as well as the solar panels. Assuming that the absorbed radiation is instantaneously reradiated into space (Fliegel et al. 1992), the radiation pressure acceleration of the satellite body surface is obtained as

$$a = -\frac{A}{M}\frac{S_0}{c}\cos\theta\left[(\alpha+\delta)\left(\vec{e}_D+\frac{2}{3}\vec{e}_N\right) + 2\rho\cos\theta\vec{e}_N\right] \tag{11}$$

The acceleration of the solar panels can be expressed by

$$a = -\frac{A}{M}\frac{S_0}{c}\cos\theta\left[(\alpha+\delta)\vec{e}_D + 2\left(\frac{\delta}{3}+\rho\cos\theta\right)\vec{e}_N\right] \tag{12}$$

Here, A is the area of the individual body or solar panel surfaces and M is the mass of satellite. S_0 is the solar flux at 1AU and c is the velocity of light. α, ρ and δ are the absorption, specular reflection and diffuse reflection coefficients of each surface. $\vec{e}_D$ is the satellite-Sun unit vector, and $\vec{e}_N$ is the unit vector normal to the body or solar panel surfaces. $\vec{e}_D$ and $\vec{e}_N$ enclose the angle $\theta = \arccos\left(\vec{e}_D^T\vec{e}_N\right)$.

According to Galileo and QZS-2 satellite metadata, several different materials are adopted for satellite bus surfaces as well as solar panels (EGSC 2017; CAO 2018). As a result, the processing of weighted averaging is performed to get the optical properties coefficients summarized in Table 3. Unlike the box-wing-hat model from Ikari et al. (2013), we simply consider the L-ANT cover of QZS-2 satellite as contribution to $+Z$ surface, and neglect its contribution to $-X$ surface. Note that QZS-1 is not considered in the analysis of SRP modeling since the optical properties are "currently investigated" (CAO 2017).

3.2 Processing strategy

To quantify the influence of new satellite metadata on Galileo and QZSS POD, datasets of 360 days during DOY 001-360 2017 are processed in different strategies. For the analysis of PCO/PCV corrections, different PCO/PCV values from DLR/GFZ and new published metadata are employed for POD. The POD performances with nominal and new modeled yaw attitude are analyzed, and two types of SRP models of ECOM2 and the proposed a priori box-wing with metadata are studied.

Table 3 Geometrical and optical properties of Galileo and QZSS satellites for the a priori box-wing SRP model

Satellites	Mass (kg)	Box-wing	Area (m^2)	Absorption	Specular reflection	Diffuse reflection
Galileo IOV	695–697	Wing	5.410*2	0.91	0.09	0.00
		+Z	3.000	0.78	0.09	0.13
		−Z	3.000	0.94	0.00	0.06
		−X	1.320	0.94	0.00	0.06
Galileo FOCe/FOC	FOCe: 661–662 FOC: 706–710	Wing	5.410*2	0.91	0.09	0.00
		+Z	3.036	0.70	0.14	0.16
		−Z	3.036	0.66	0.23	0.11
		−X	1.320	0.93	0.00	0.07
QZS-2	2324.20	Wing	14.900*2	0.92	0.07	0.01
		+Z	5. 600	0.73	0.07	0.20
		−Z	5. 600	0.93	0.03	0.04
		−X	10.100	0.93	0.03	0.04

The arc length of POD is 72 h with 5 min sampling interval. For any two adjacent three-day solutions shifted by 1 or 2 days, there are 48-h or 24-h orbit overlap errors. In this study, the 24-h orbit overlap is used to validate the POD results. The prior precisions are set to 2 m and 2 mm for raw code and carrier-phase observations, respectively. Ionosphere-free code (PC) and carrier-phase (LC) combinations are used to eliminate the first-order ionospheric delays, and the influence of high-order ionosphere terms is neglected. The weights of observations depend on elevation, and the cutoff elevation is set to 7°. Due to the lack of a complete and consistent set of Galileo receiver antenna calibrations, the GPS L2 PCOs and PCVs are also applied for Galileo E5a. This appears to be reasonable since only small differences were reported for the adjacent L2 and E5a frequency bands (Becker et al. 2010). GPS are processed together with Galileo and QZSS to improve the solution strength. The detailed information about observational models, dynamical modes and estimated parameters are summarized in Table 4.

4 POD results with the new metadata

4.1 PCO and PCV corrections

In order to evaluate the influence of the antenna PCO and PCV included in the new metadata on Galileo orbit determination, the MGEX data of DOY 001-360 2017 are

Table 4 Observational models, dynamical models and estimated parameters for Galileo and QZSS POD

Items	Models
Software	Position And Navigation Data Analyst (PANDA) software (Liu and Ge 2003)
Basic observables	Galileo: E1 + E5a ionosphere-free code and phase combination QZSS: L1 + L2 ionosphere-free code and phase combination GPS: L1 + L2 ionosphere-free code and phase combination
Sampling rate	300 s
Arc length	3 days
Elevation cutoff	7°
Weight for observations	Elevation-dependent weight. 1 for E > 30 ° otherwise 2*sin(*E*)
Geopotential	EGM2008 model (Pavlis et al. 2012) up to 12 × 12
N-body gravity	JPL DE421 (Folkner et al. 2009)
Solar radiation	ECOM2 versus ECOM + the a priori box-wing with metadata
Station displacement	Solid Earth tides, pole tides, ocean tide loading, International Earth Rotation and Reference System Service (IERS) conventions, 2010 (Petit and Luzum 2010); FES2004 (Lyard et al. 2006) for ocean tides
Relativistic effects	IERS conventions 2010
Phase wind-up	Corrected (Wu et al. 1993)
Satellite antenna PCO	Galileo: DLR/GFZ values (igs14_1958.atx) versus metadata values (igs14_1986.atx) QZSS: metadata values
Satellite antenna PCV	Galileo: ignored (igs14_1958.atx) versus metadata values (igs14_1986.atx) QZSS: ignored for QZS-1 and metadata values for QZS-2
Receiver antenna PCO/PCV	Corrections for GPS L1 and L2 are used for Galileo/QZSS E1/L1 and E5a/L2, respectively
Tropospheric delay	A priori zenith path delays (ZPDs) computed with formula of Saastamoinen (1973) using the Global Pressure and Temperature (GPT; Boehm et al. 2007) model; ZPDs mapped into slant delays using hydrostatic Global Mapping Function (GMF; Boehm et al. 2006); the residual tropospheric delays estimated as piecewise constant function with 2-h ZPDs and 24-h gradients parameter spacing using the wet GMF
Antenna thrust	Galileo transmit power: 135 W for IOV E11 and E12, 95 W for IOV E19; 265 W for FOCe and FOC satellites (Steigenberger et al. 2017) QZSS transmit power: 250 W for QZS-1 and 500 W for QZS-2 (CAO 2017, 2018)
Station coordinates	The initial values are set to the IGS14 coordinates from IGS weekly combined solution; estimated with tight constraints using the standard deviations from IGS weekly combined solution
Receiver clocks	Epoch-wise estimated as white noise; Inter-system biases (ISBs) of Galileo/QZSS w.r.t. GPS are estimated as constants for each receiver
Satellite clocks	Epoch-wise estimated as white noise
Phase ambiguities	Real constant for each ambiguity arc; DD AR is implemented separately for GPS, Galileo and QZSS
ERP parameters	Offsets and drifts (X_{pole}, dX_{pole}, Y_{pole}, DY_{pole}, UT1 and DUT1) are estimated every 3-day POD arc; UT1 is tightly constrained
SRP parameters	ECOM2: 9 parameters in Eq. (9) The a priori box-wing: 5 ECOM parameters (Springer et al. 1999)

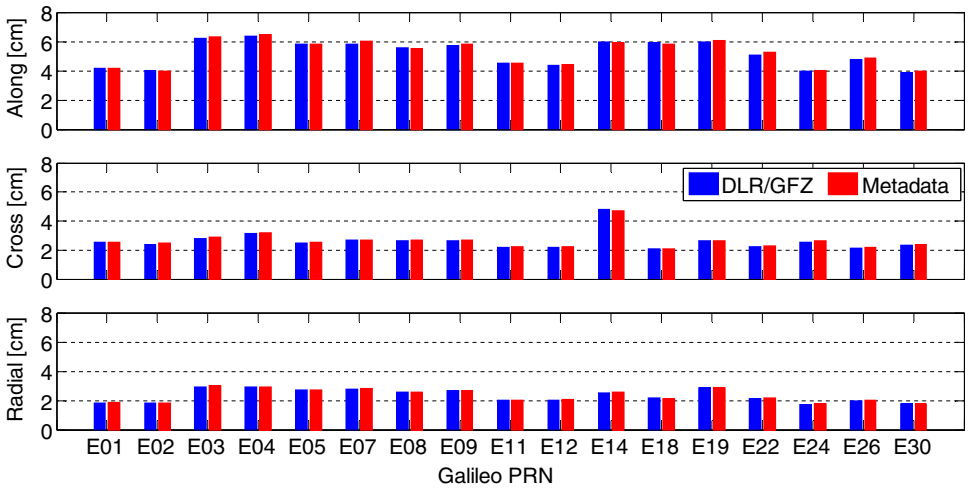

Fig. 4 Galileo orbit overlap RMS using PCO/PCV from DLR/GFZ and new metadata. ECOM2 9 parameter SRP model is used here

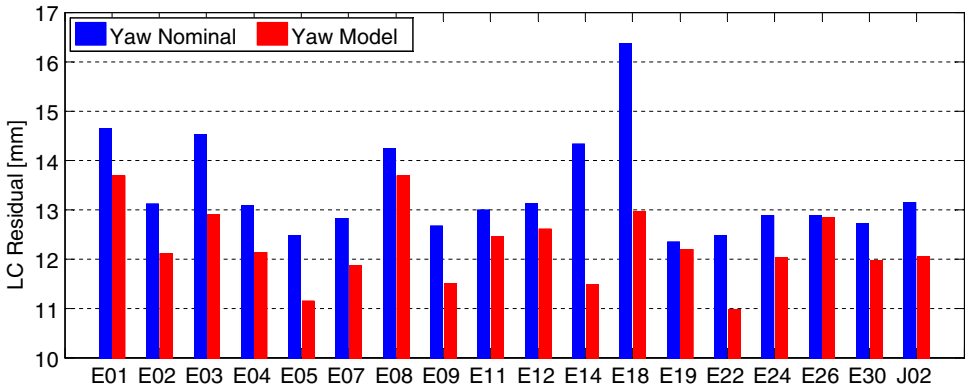

Fig. 5 The RMS values of LC residuals for Galileo and QZSS satellites during noon-turn and midnight-turn maneuvers. The thresholds of orbital angles are $|\mu| < 15°$ or $|\mu - 180°| < 15°$ for IOV satellites, $|\mu| < 9.1°$ or $|\mu - 180°| < 9.1°$ for FOCe and FOC satellites and $\mu \in (\mu_s, \mu_e)$ for QZS-2. The SRP model is ECOM2

processed using the DLR/GFZ PCOs (no PCVs available) and the PCO/PCV values from the new metadata, respectively. In our processing, ECOM2 SRP model is applied.

The RMS values of Galileo orbit 24-h overlap using different PCO/PCV corrections are presented in Fig. 4. We can find that the POD results based on PCO/PCVs from the new metadata have a generally comparable performance in all the three components to those based on DLR/GFZ values, with the differences within 1 mm. The 3D orbit overlaps applying the new metadata PCO/PCVs are 0.7 and 0.8 mm larger for the IOV and FOC satellites, respectively, while 0.9 mm smaller for the FOCe satellites. Similar differences of 3D overlap can be observed when the a priori box-wing model is applied. With this model, the POD results using new metadata PCO/PCVs have 0.1 and 0.5 mm larger RMS for IOV and FOC but 1.2 mm smaller RMS for FOCe. Updating the antenna calibrations has only a limited impact on the orbits. It is possible since the two sets of PCOs mainly differ in the z-component, which is highly correlated with satellite clock bias. The statistics show that almost all of the z-PCO differences can be compensated by satellite clock estimates. We still use the new metadata PCO/PCVs in the following experiments to keep consistent with the latest ANTEX file.

Table 5 3D overlap RMS (in unit of cm) of Galileo and QZSS satellites during/outside eclipse seasons

Satellites	IOV	FOCe	FOC	QZS-2
Outside	5.95	7.27	6.11	19.24
Yaw nominal	12.28	16.79	14.68	34.66
Yaw model	11.68	15.84	13.41	32.92

4.2 Attitude law

The observation residuals will absorb the errors caused by the inaccurate yaw-attitude model and thus can be used to analyze the influence of the new yaw-attitude law on

Galileo and QZSS POD. The RMS values of LC observation residuals for all Galileo and QZS-2 satellites during noon-turn and midnight-turn maneuvers are shown in Fig. 5. The blue bars are for nominal yaw-attitude model, and the red bars are for new yaw-attitude model. The comparison also reveals that the new yaw-attitude model can obviously reduce the LC residuals during noon- and midnight-turns. It is worth noting that Galileo FOC attitude law also works well for the FOCe satellites.

Table 5 summarizes the 3D overlap RMS of Galileo and QZS-2 satellites during/outside the eclipse seasons. For IOV, FOCe, FOC and QZS-2 satellites, the new yaw-attitude model can reduce the overlap RMS values during the eclipse seasons from 12.3 cm, 16.8 cm, 14.7 cm and 34.7 cm to 11.7 cm, 15.8 cm, 13.4 cm and 32.9 cm, respectively. Again the Galileo FOC attitude law works well for the FOCe satellites. It is possible that FOCe satellites still use FOC attitude control model although they are in elliptical orbits, which needs further confirmation with EGSC. However, the 3D overlap RMS values during eclipse seasons are still much larger than those outside eclipse seasons. The orbit modeling for eclipsing satellites is typically the most challenging, as the Sun illuminates the three surfaces of the satellite body, and the illuminated cross-sectional area varies most (Sośnica et al. 2017).

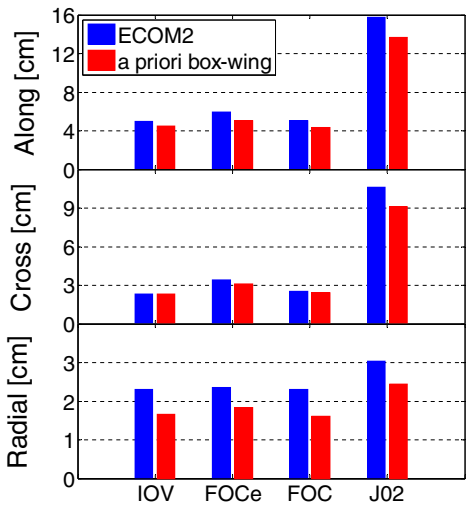

Fig. 6 Galileo and QZSS orbit overlap RMS using different SRP models

4.3 SRP models

Figure 6 illustrates the orbit overlap RMS values when the ECOM2 and the proposed a priori box-wing SRP models are applied. For Galileo IOV, FOCe and FOC satellites, the 3D RMS values of the proposed a priori box-wing model are 5.3 cm, 6.2 cm and 5.3 cm, respectively, which are 11.0%, 14.7% and 14.0% smaller than those of ECOM2. This may be attributed to the accurate dimensions and optical properties from the new metadata. It is worth noting that the a priori box-wing model also works well for FOCe satellites with elliptical orbits. For QZS-2, we can find that the a priori box-wing model shows the better 3D overlap RMS values of 16.6 cm with an improvement of 13.8% compared with ECOM2. Nevertheless, the POD performance of QZS-2 is inferior to that of Galileo satellites, especially in the along-track and cross-track components. This indicates that deficiencies still exist in QZS-2 SRP modeling, which needs further investigations.

Since all Galileo and QZSS satellites are equipped with laser retro-reflector arrays (Dell'Agnello et al. 2010) and tracked by the International Laser Ranging Service (ILRS; Pearlman et al. 2002) on an operational basis, one-way satellite laser ranging (SLR) residuals are also applied to evaluate the performance of the SRP models. The ILRS site coordinates and velocities as well as site eccentricities based on the International Terrestrial Reference Frame ITRF2014 (Altamimi et al. 2016) are used for the SLR stations. The station displacement models, including solid Earth tides, ocean tidal loading and the mean pole definition, are consistent with the IERS conventions 2010 (Petit and Luzum 2010). To correct the range measurements for atmospheric refraction, the tropospheric delays were modeled using the Mendes and Pavlis model (Mendes and Pavlis 2004). The LRA offset values provided by Galileo and QZSS metadata have been applied in order to refer the SLR observations to the spacecraft's center of mass. The SLR measurements with range residuals exceeding values of 20 cm and 30 cm were excluded from the residual analysis for Galileo and QZSS, respectively.

The SLR validation results are summarized in Table 6. The SLR residuals applying the a priori box-wing model present the smaller mean bias for FOCe, FOC and QZS-2, which are −0.4 cm, −0.4 cm and 0.6 cm, whereas slightly larger mean bias of −1.0 cm is observed for Galileo IOV

Table 6 SLR results of Galileo and QZSS satellites using different SRP models (in cm)

Satellites	Galileo IOV		Galileo FOCe		Galileo FOC		QZS-2	
	Mean bias	STD	Mean bias	STD	Mean bias	STD	Mean bias	STD
ECOM2	0.5	3.8	1.1	3.5	1.2	4.1	−1.7	4.9
The a priori box-wing	−1.0	3.4	−0.4	3.1	−0.4	3.4	0.6	4.7

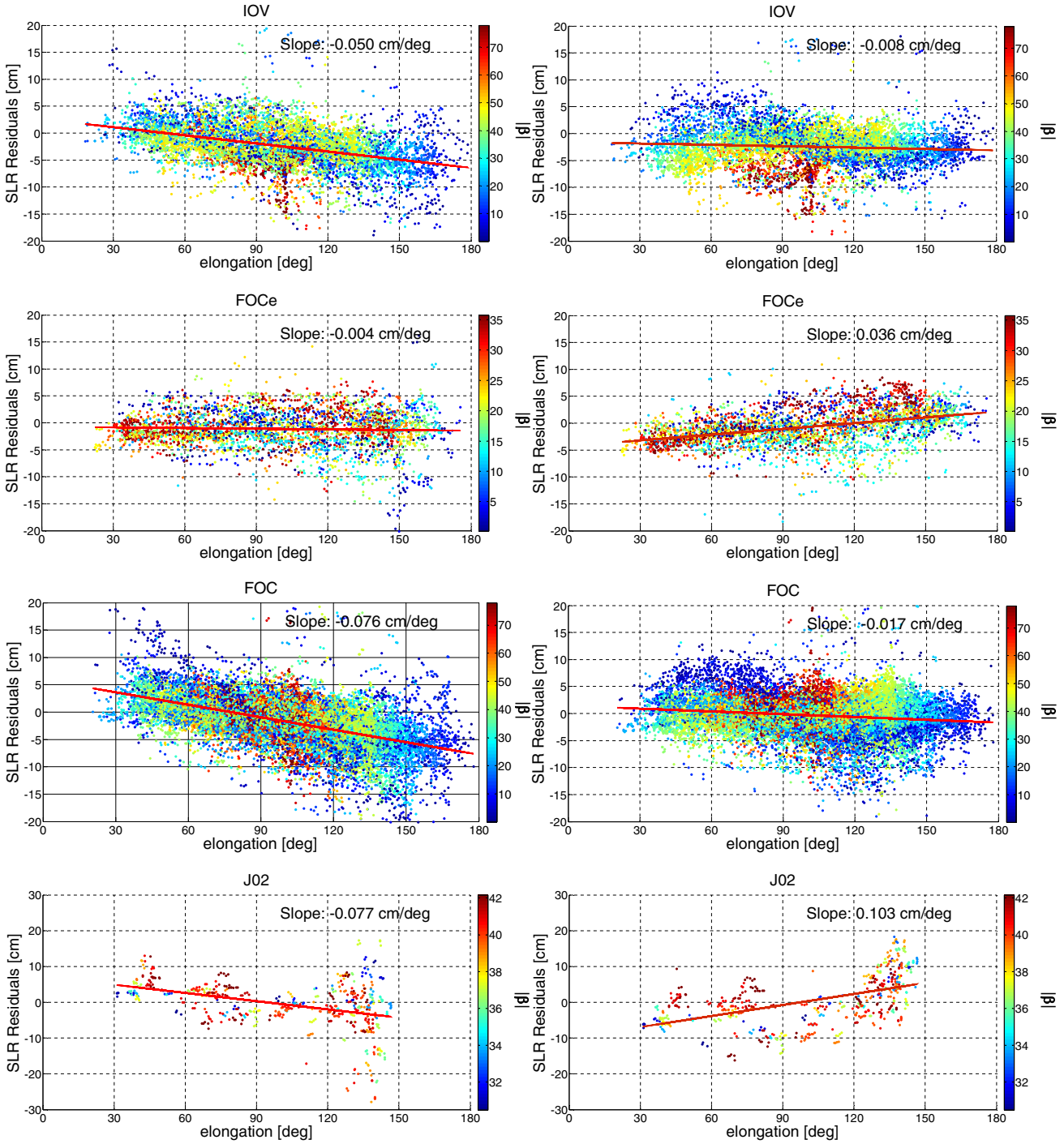

Fig. 7 Dependency of SLR residuals on the satellite elongation angle w.r.t. the Sun when using ECOM2 and the a priori box-wing model with metadata. The left subfigures are the SLR residuals using ECOM2 SRP model, while the right subfigures are those using the a priori box-wing model with metadata

satellites. The SLR residuals using the a priori box-wing model with metadata show the smaller STD of 3.4 cm, 3.1 cm, 3.4 cm and 4.7 cm for IOV, FOCe, FOC and QZS-2, respectively. When compared to the CBW model by Montenbruck et al. (2015b) and Steigenberger and Montenbruck (2016), the a priori box-wing model with detailed dimensions and optical properties also presents 0.1 cm and 0.1 cm smaller STD values for FOCe and FOC satellites, while the STD value of IOV satellites is 0.2 cm larger.

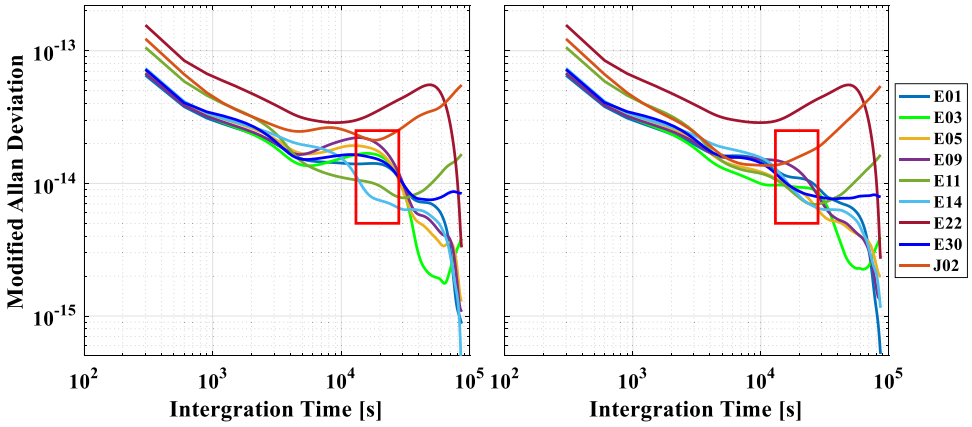

Fig. 8 Modified Allan Deviations of Galileo and QZS-2 clocks in DOY 244 2017. The left subfigure is clocks with ECOM2 model, and the right subfigure is the a priori box-wing with new metadata

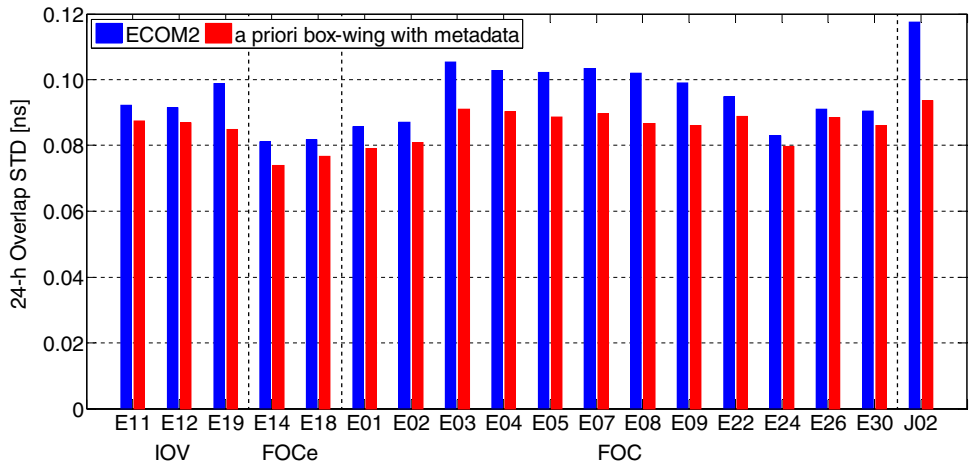

Fig. 9 STD values of 24-h clock overlap for Galileo and QZSS satellites

In Fig. 7 we also examine the SLR residuals as a function of the satellite–Sun elongation angle ε:

$$\cos\varepsilon = \cos\beta\cos\Delta u. \tag{13}$$

Figure 7 shows that, with SRP model of ECOM2, Galileo IOV and FOC satellites exhibit SLR residual dependencies on the elongation angle. The slopes are -0.50 mm/° and -0.76 mm/° for IOV and FOC satellites, respectively. When the a priori box-wing SRP model is applied, these residual dependencies almost vanish, with the slopes being -0.08 mm/° for IOV and -0.17 mm/° for FOC. However, for Galileo FOCe satellites with ECOM2 model, none dependency of SLR residuals on the elongation angle is observed, which is different to the result of the period 2014.0–2016.5 in Sośnica et al. (2017). We have checked the Galileo orbits of 2017 provided by CODE, and also none elongation-dependency can be found. For QZS-2, SLR residual dependency can also be found in ECOM2 model with a slope of -0.77 mm/°. Nevertheless, the using of the a priori box-wing model cannot reduce the elongation-dependency but increases the absolute value of the slope by almost 50%, which needs further investigation since the number of QZS-2 SLR observations is much less than that of Galileo.

5 Clock performance with the new metadata

The Galileo satellites are equipped with two RAFSs and two PHMs for all IOV and FOC satellites (Steigenberger and Montenbruck 2016), while the QZSS satellites are running on RAFSs (http://qzss.go.jp/en/technical/satellites/index.html#QZSS). To assess Galileo and QZSS onboard satellite clocks with different solutions, the Modified Allan deviation (MADEV) is computed from the 300 s sampling clocks. The outliers, clock and frequency jumps as well as day-boundary discontinuities are carefully examined and removed before the analysis. The median absolute deviation method using 3-sigma is performed to detect and remove the outliers.

Figure 8 shows the Galileo and QZSS clock stability in DOY 244 2017. It can be found that E11, E22 and QZS-2

clocks show the worst performance for integration times longer than 40,000 s, which is reasonable due to that they were running on RAFSs. For Galileo FOC satellites, the PHM clocks applying ECOM2 model (left subfigure) exhibit obvious bumps for integration time at 20,000 s. However, these bumps almost disappear in PHM clocks using the a priori box-wing model with metadata (right subfigure). When ECOM2 is applied, the averaged stability of 20,000 s is 1.68×10^{-14} for Galileo FOC satellites, while it is decreased by 0.43×10^{-14} after applying the a priori box-wing model with metadata, with a significant improvement of 25.6%. The other PHM clocks exhibit similar performance with the examples shown in Fig. 8.

In order to further evaluate the influence of new metadata on clocks, the STD values of 24-h clock overlap are calculated and shown in Fig. 9. It can be seen that the mean overlap STD values of clocks applying ECOM2 are 0.094 ns, 0.081 ns, 0.095 ns and 0.117 ns for IOV, FOCe, FOC and QZS-2 satellites, respectively. When the a priori box-wing model and the new metadata are applied, the mean overlap STDs can be reduced to 0.086 ns, 0.075 ns, 0.086 ns and 0.093 ns, respectively, with improvements of 8.5%, 7.4%, 9.5% and 20.5%.

6 Conclusions

In this contribution, the benefits of new satellite metadata to Galileo and QZSS orbit and clock determination are studied. Several updates are implemented, including PCO/PCV corrections, yaw-attitude models and SRP models. The observations of DOY 001-360 2017 are processed for detailed analysis and evaluations.

Compared to the DLR/GFZ values with only PCO corrections, the using of the PCO/PCV from new metadata leads to comparable orbit overlap RMS. The limited influence of PCO/PCVs on Galileo orbit can be attributed to the high correlations between z-PCOs and satellite clock biases, since the two sets of PCOs mainly differ in the z-component. The Galileo and QZS-2 yaw-attitude laws included in the satellite metadata are applied in Galileo and QZS-2 POD. Compared with the nominal yaw-attitude model, the new yaw-attitude model can obviously reduce the LC residuals during noon- and midnight-turns. With the new attitude model, the overlap RMS in eclipsing seasons can be decreased from 12.3 cm, 16.8 cm, 14.7 cm and 34.7 cm to 11.7 cm, 15.8 cm, 13.4 cm and 32.9 cm for Galileo IOV, FOCe, FOC and QZS-2 satellites, respectively. With the accurate satellite dimensions and optical properties, the 3D orbit overlap RMS values of the a priori box-wing SRP model are 5.3 cm, 6.2 cm, 5.3 cm and 16.6 cm for Galileo IOV satellites, FOCe satellites, FOC satellites and QZS-2, respectively, with improvements of 11.0%, 14.7%, 14.0% and 13.8% compared with those of ECOM2. Meanwhile, the a priori box-wing model presents either the smaller SLR STDs or the smaller SLR mean biases except Galileo IOV satellites. In addition, the a priori box-wing model helps to eliminate the SLR residual dependencies of Galileo IOV and FOC satellites on the elongation angle.

Besides, the performances of Galileo and QZSS onboard satellite clocks are also assessed. When ECOM2 is applied, visible bumps appear in the MADEV of Galileo PHMs for integration time at 20,000 s. These bumps almost vanish in PHMs with the a priori box-wing model and new metadata. The clock overlap STD values can also be improved by 8.5%, 7.4%, 9.5% and 20.5% for IOV, FOCe, FOC and QZS-2 when applying the a priori box-wing model.

In summary, the release of new satellite metadata is helpful for the GNSS community. Updating yaw-attitude models when $|\beta| \approx 0$ and using the a priori box-wing SRP model together with detailed satellite dimensions as well as optical properties can improve the performances of Galileo/QZSS orbits and clocks. The influences of Earth albedo, which is neglected in this study, need further investigation in future works. As a result of the lower mass compared to GPS/GLONASS/BeiDou/QZSS, the albedo is expected to have a larger impact on Galileo orbit (Montenbruck et al. 2017). Meanwhile, the performances of orbits and clocks may also be improved for other GNSS if the metadata of these satellites can be disclosed (Montenbruck and on behalf of the IGS Multi-GNSS Working Group 2017), including the new BeiDou as well as the modernized GLONASS satellites.

Acknowledgements We are very grateful to the International GNSS Service (IGS) and the International Laser Ranging Service (ILRS) for providing GNSS and SLR observation data. This study is financially supported by the National Natural Science Foundation of China (Grant No. 41774030), the Hubei Province Natural Science Foundation of China (Grant No. 2018CFA081) and the National Youth Thousand Talents Program.

References

Altamimi Z, Rebischung P, Métivier L et al (2016) ITRF2014: a new release of the International Terrestrial Reference Frame modeling nonlinear station motions. J Geophys Res Solid Earth 121(8):6109–6131. https://doi.org/10.1002/2016JB013098

Arnold D, Meindl M, Beutler G et al (2015) CODE's new solar radiation pressure model for GNSS orbit determination. J Geod 89(8):775–791. https://doi.org/10.1007/s00190-015-0814-4

Bar-Sever Y (1994) New GPS attitude model. In: IGSMAIL-0591. IGS Central Bureau, Pasadena

Bar-Sever Y, Kuang D (2004) New empirically derived solar radiation pressure model for global positioning system satellites. IPN progress report pp 42–159, Nov 15, 2004

Becker M, Zeimetz P, Schönemann E (2010) Anechoic chamber calibrations of phase center variations for new and existing GNSS

signals and potential impacts in IGS processing. In: IGS workshop 2010, Newcastle
Beutler G, Brockmann E, Gurtner W et al (1994) Extended orbit modeling techniques at the CODE processing center of the international GPS service for geodynamics(IGS): theory and initial results. Manuscr Geod 19(6):367–386
Boehm J, Niell A, Tregoning P et al (2006) Global Mapping Function (GMF): a new empirical mapping function based on numerical weather model data. Geophys Res Lett. https://doi.org/10.1029/2005gl025546
Boehm J, Heinkelmann R, Schuh H (2007) Short note: a global model of pressure and temperature for geodetic applications. J Geod 81(10):679–683. https://doi.org/10.1007/s00190-007-0135-3
Dach R, Schaer S, Arnold D et al (2016) CODE analysis center technical report 2015. In: Jean Y, Dach R (eds) International GNSS service: technical report 2015, (AIUB), IGS Central Bureau and University of Bern, Bern Open Publishing, pp 25–44, June 2016. https://doi.org/10.7892/boris.80307
de Selding PB (2014) ESA proceeding with Galileo launches despite in-orbit satellite issues. SpaceNews. http://spacenews.com/41616esa-proceeding-with-galileo-launches-despite-in-orbitsatellite-issues. Accessed 10 May 2016
Dell'Agnello SD et al (2010) Creation of the new industry-standard space test of laser retroreflectors for the GNSS and LAGEOS. Adv Space Res 47(5):822–842. https://doi.org/10.1016/j.asr.2010.10.022
Dilssner F (2010) GPS IIF-1 satellite, antenna phase center and attitude modeling. Inside GNSS 5(6):59–64
Dilssner F, Springer T, Gienger G et al (2011) The GLONASS-M satellite yaw-attitude model. Adv Space Res 47(1):160–171. https://doi.org/10.1016/j.asr.2010.09.007
Dow JM, Neilan R, Rizos C (2009) The International GNSS Service in a changing landscape of global navigation satellite systems. J Geod 83(3–4):191–198. https://doi.org/10.1007/s00190-008-0300-3
European GNSS Service Centre (EGSC) (2017) Galileo satellite metadata. https://www.gsc-europa.eu/support-to-developers/galileo-satellite-metadata. Accessed 10 Jan 2018
Fliegel HF, Gallini TE, Swift ER (1992) Global positioning system radiation force model for geodetic applications. J Geophys Res 97(B1):559–568. https://doi.org/10.1029/91JB02564
Folkner WM, Williams JG, Boggs DH (2009) The planetary and lunar ephemeris DE 421. Technical report IPN progress report, pp 42–178. Jet Propulsion Laboratory
Guo J, Chen G, Zhao Q et al (2016) Comparison of solar radiation pressure models for BDS IGSO and MEO satellites with emphasis on improving orbit quality. GPS Solut 21(2):511–522. https://doi.org/10.1007/s10291-016-0540-2
Hauschild A, Steigenberger P, Rodriguez-Solano C (2012) Signal, orbit and attitude analysis of Japan's first QZSS satellite Michibiki. GPS Solut 16:127–133. https://doi.org/10.1007/s10291-011-0245-5
Ikari S, Ebinuma T, Funase R et al (2013) An evaluation of solar radiation pressure models for QZS-1 precise orbit determination. In: Proceedings of ION GNSS. ION, Nashville, pp 1234–1241
Ishijima Y, Inaba N, Matsumoto A et al (2009) Design and development of the first Quasi-Zenith Satellite attitude and orbit control system. In: 2009 IEEE aerospace conference. IEEE, pp 1–8. https://doi.org/10.1109/aero.2009.4839537
Kogure S (2012) QZSS antenna coordinates; eMail to Montenbruck O, 2012/07/20
Kouba J (2008) A simplified yaw-attitude model for eclipsing GPS satellites. GPS Solut 13(1):1–12. https://doi.org/10.1007/s10291-008-0092-1
Kouba J (2013) Noon turns for deep eclipsing Block IIF GPS satellites, a note prepared for IGS ACs, dated 19 Dec 2013 [IGS-ACS-930 Mail]
Liu J, Ge M (2003) PANDA software and its preliminary result of positioning and orbit determination. Wuhan Univ J Nat Sci 8(2B):603–609. https://doi.org/10.1007/BF02899825
Lyard F, Lefevre F, Letellier T et al (2006) Modelling the global ocean tides: modern insights from FES2004. Ocean Dyn 56(5–6):394–415. https://doi.org/10.1007/s10236-006-0086-x
Meindl M, Beutler G, Thaller D et al (2013) Geocenter coordinates estimated from GNSS data as viewed by perturbation theory. Adv Space Res 51(7):1047–1064. https://doi.org/10.1016/j.asr.2012.10.026
Mendes VB, Pavlis EC (2004) High-accuracy zenith delay prediction at optical wavelengths. Geophys Res Lett. https://doi.org/10.1029/2004gl020308
Montenbruck O, on behalf of the IGS Multi-GNSS Working Group (2017) IGS white paper on satellite and operations information for generation of precise GNSS orbit and clock products. Version 2017/10/21
Montenbruck O, Steigenberger P, Khachikyan R et al (2014) IGS-MGEX: preparing the ground for multi-constellation GNSS science. Inside GNSS 9(1):42–49
Montenbruck O, Schmid R, Mercier F et al (2015a) GNSS satellite geometry and attitude models. Adv Space Res 56:1015–1029. https://doi.org/10.1016/j.asr.2015.06.019
Montenbruck O, Steigenberger P, Hugentobler U (2015b) Enhanced solar radiation pressure modeling for Galileo satellites. J Geod 89(3):283–297. https://doi.org/10.1007/s00190-014-0774-0
Montenbruck O, Steigenberger P, Prange L et al (2017) The multi-GNSS experiment (MGEX) of the international GNSS service (IGS): achievements, prospects and challenges. Adv Space Res 59(7):1671–1697. https://doi.org/10.1016/j.asr.2017.01.011
Pavlis NK, Holmes SA, Kenyon SC et al (2012) The development and evaluation of the earth gravitational model 2008 (EGM2008). J Geophys Res Solid Earth 117:B04406. https://doi.org/10.1029/2011JB008916
Pearlman MR, Degnan JJ, Bosworth JM (2002) The international laser ranging service. Adv Space Res 30(2):135–143. https://doi.org/10.1016/S0273-1177(02)00277-6
Petit G, Luzum B (2010) IERS conventions 2010. No. 36 in IERS technical note, Verlag des Bundesamts für Kartographie und Geodäsie, Frankfurt am Main, Germany
Prange L, Dach R, Lutz S et al (2016) The CODE MGEX orbit and clock solution. In: Rizos C, Willis P (eds), IAG 150 years, international association of geodesy symposia, vol 143. Springer, pp 767–773. https://doi.org/10.1007/1345_2015_161
Prange L, Orliac E, Dach R et al (2017) CODE's five-system orbit and clock solution: the challenges of multi-GNSS data analysis. J Geod 91(4):345–360. https://doi.org/10.1007/s00190-016-0968-8
Rodríguez-Solano C, Hugentobler U, Steigenberger P et al (2014) Reducing the draconitic errors in GNSS geodetic products. J Geod 88(6):559–574. https://doi.org/10.1007/s00190-014-0704-1
Saastamoinen J (1973) Contributions to the theory of atmospheric refraction. Bull Géod 107(1):13–34. https://doi.org/10.1007/BF02522083
Schmid R, Rothacher M, Thaller D et al (2005) Absolute phase center corrections of satellite and receiver antennas: impact on global GPS solutions and estimation of azimuthal phase center variations of the satellite antenna. GPS Solut 9(4):283–293. https://doi.org/10.1007/s10291-005-0134-x
Schmid R, Steigenberger P, Gendt G et al (2007) Generation of a consistent absolute phase-center correction model for GPS receiver and satellite antennas. J Geod 81(12):781–798. https://doi.org/10.1007/s00190-007-0148-y
Schmid R, Dach R, Collilieux X et al (2015) Absolute IGS antenna phase center model igs08.atx: status and potential improvements. J Geod 90(4):343–364. https://doi.org/10.1007/s00190-015-0876-3

Sośnica K, Prange L, Kaźmierski K et al (2017) Validation of Galileo orbits using SLR with a focus on satellites launched into incorrect orbital planes. J Geod 92(12):131–148. https://doi.org/10.1007/s00190-017-1050-x

Springer TA, Beutler G, Rothacher M (1999) A new solar radiation pressure model for GPS satellites. GPS Solut 3(2):50–62. https://doi.org/10.1007/PL00012757

Steigenberger P, Montenbruck O (2016) Galileo status: orbits, clocks, and positioning. GPS Solut 21(2):319–331. https://doi.org/10.1007/s10291-016-0566-5

Steigenberger P, Dach R, Prange L et al (2015) Galileo satellite antenna modeling. In: Geophys research abstract, vol 17, EGU2015-10772-1

Steigenberger P, Fritsche M, Dach R et al (2016) Estimation of satellite antenna phase center offsets for Galileo. J Geod 90(8):773–785. https://doi.org/10.1007/s00190-016-0909-6

Steigenberger P, Thoelert S, Montenbruck O et al (2017) GNSS satellite transmit power and its impact on orbit determination. J Geod 92(6):609–624. https://doi.org/10.1007/s00190-017-1082-2

The Cabinet Office Government of Japan (2017) QZS-1 satellite information (SPI-QZS1) http://qzss.go.jp/en/technical/qzssinfo/khp0mf0000000wuf-att/spi_qzs1.pdf?t=1528617014169. Accessed 31 May 2018

The Cabinet Office Government of Japan (2018) QZS-2/3/4 satellite information (SPI-QZS2_B/SPI-QZS3_A/SPI-QZS4_B) http://qzss.go.jp/en/technical/qzssinfo/khp0mf0000000wuf-att/spi-qzs2_b.pdf?t=1528617014170; http://qzss.go.jp/en/technical/qzssinfo/khp0mf0000000wuf-att/spi-qzs3_a.pdf?t=1528682820729; http://qzss.go.jp/en/technical/qzssinfo/khp0mf0000000wuf-att/spi-qzs4_b.pdf?t=1528682820729. Accessed 31 May 2018

Wu J, Wu S, Hajj G et al (1993) Effects on antenna orientation on GPS carrier phase. Manuscr Geod 18(2):91–98

Zhao Q, Chen G, Guo J et al (2017) An a priori solar radiation pressure model for the QZSS Michibiki satellite. J Geod 92(8):1–13. https://doi.org/10.1007/s00190-017-1048-4